Acta Crystallographica Section D
Biological Crystallography
ISSN 0907-4449

Urate oxidase from *Aspergillus flavus*: new crystal-packing contacts in relation to the content of the active site

Pascal Retailleau,[a,b]* Nathalie Colloc'h,[c] Denis Vivarès,[d,e] Françoise Bonneté,[d] Bertrand Castro,[f] Mohamed El Hajji[f] and Thierry Prangé[a,g]

[a]LURE, Centre Universitaire Paris-Sud, Bâtiment 209D, BP 34, 91898 Orsay CEDEX, France, [b]Institut de Chimie des Substances Naturelles (CNRS), 1 Avenue de la Terrasse, 91198 Gif sur Yvette CEDEX, France, [c]UMR 6185 CNRS, Université de Caen, Centre Cyceron, Boulevard Becquerel, BP 5229, 14074 Caen CEDEX, France, [d]CRMCN (UPR 7251 CNRS), Campus de Luminy, Case 913, 13288 Marseille CEDEX 09, France, [e]Laboratoire de Bioénergétique Cellulaire, UMR 6191, CEA Cadarache, 13108 Saint-Paul-lez-Durance CEDEX, France, [f]Sanofi–Aventis, 82 Avenue Raspail, 94255 Gentilly CEDEX, France, and [g]Laboratoire de Cristallographie et RMN Biologiques (UMR 8015 CNRS), Faculté de Pharmacie, Université Paris V, 4 Avenue de l'Observatoire, 75270 Paris CEDEX 06, France

Correspondence e-mail: pascal.retailleau@icsn.cnrs-gif.fr

Received 1 October 2004
Accepted 29 November 2004

PDB References: Uox–uracil complex, 1ws3, r1ws3sf; Uox–5,6-diaminouracil complex, 1ws2, r1ws2sf; Uox–5-amino 6-nitrouracil complex, 1wrr, r1wrrsf; 1xxj, r1xxjsf; Uox–guanine complex, 1xy3, r1xy3sf; Uox–guanine complex, 1xt4, r1xt4sf.

Urate oxidase from *Aspergillus flavus* (uricase or Uox; EC 1.7.3.3) is a 135 kDa homotetramer with a subunit consisting of 301 amino acids. It catalyses the first step of the degradation of uric acid into allantoin. The structure of the extracted enzyme complexed with a purine-type inhibitor (8-azaxanthin) had been solved from high-resolution X-ray diffraction of *I*222 crystals. Expression of the recombinant enzyme in *Saccharomyces cerevisiae* followed by a new purification procedure allowed the crystallization of both unliganded and liganded enzymes utilizing the same conditions but in various crystal forms. Here, four different crystal forms of Uox are analyzed. The diversity of the Uox crystal forms appears to depend strongly on the chemicals used as inhibitors. In the presence of uracil and 5,6-diaminouracil crystals usually belong to the trigonal space group $P3_121$, the asymmetric unit (AU) of which contains one tetramer of Uox (four subunits). Chemical oxidation of 5,6-diaminouracil within the protein may occur, leading to the canonical (*I*222) packing with one subunit per AU. Coexistence of two crystal forms, $P2_1$ with two tetramers per AU and *I*222, was found in the same crystallization drop containing another inhibitor, guanine. Finally, a fourth form, $P2_12_12$ with one tetramer per AU, resulted fortuitously in the presence of cymelarsan, an additive. Of all the reported forms, the *I*222 crystal forms present by far the best X-ray diffraction resolution (∼1.6 Å resolution compared with 2.3–3.2 Å for the other forms). The various structures and contacts in all crystalline lattices are compared. The backbones are essentially conserved except for the region near the active site. Its location at the dimer interface is thus likely to be at the origin of the crystal contact changes as a response to the various bound inhibitors.

1. Introduction

Urate oxidase is an enzyme of therapeutic interest that is implicated in the catalysed degradation of uric acid into allantoin. It has been produced by Sanofi from *Aspergillus flavus* according to a patented process and was poised to crystallize at the outcome of the purification column, a putative reminiscence of its ability to form crystalloid cores in mammalian livers (Alvares *et al.*, 1992). The first three-dimensional structure of Uox was solved at 2.05 Å resolution in complex with 8-azaxanthin, a stabilizing inhibitor (Colloc'h *et al.*, 1997). Owing to its availability and its ability to crystallize in polyethylene glycol (PEG), Uox became an eligible candidate for crystallogenesis studies, allowing Bonneté and coworkers to propose a new model for large proteins crys-

tallizing in the presence of PEG (Bonneté *et al.*, 2001; Vivarès & Bonneté, 2002). It is noteworthy that all these studies referred to the original crystal form belonging to space group *I*222 since the enzyme was always supplied with its inhibitor (8-azaxanthin). Recently, expression of recombinant enzyme in *Saccharomyces cerevisiae* by Sanofi–Aventis allowed us to work with unliganded enzyme, which was able to crystallize, albeit in a different form, under standard crystal-growth conditions (Vivarès & Bonneté, 2002). Hence, it became possible to test new inhibitor bindings in order to document the topology of the active site and to possibly shed new light on the original oxidation mechanism of Uox. Reports of Uox structures complexed with 8-azaxanthin, 9-methyluric acid or oxonic acid are available in Retailleau *et al.* (2004), which also describes the structure of the ligand-free enzyme solved in a monoclinic form ($P2_1$).

We set up cocrystallizations with a set of compounds comprising pyrimidines (uracil and 5,6-diaminouracil) and a purine (guanine) as potential inhibitors. 5,6-Diaminouracil is a slow alternative substrate for hydroxyisourate hydrolase, which has been shown to relay Uox in the uric acid metabolism cascade (Raychaudhuri & Tipton, 2003). A new trigonal crystal form characterized as $P3_121$ is induced in the presence of pyrimidines, whereas guanine was found to favour not only the $P2_1$ form but also the canonical *I*222 form. Since the tetrameric conformation is strictly conserved in all the crystal forms, transition between them is likely to involve subtle rearrangements within the active site to induce variations at the level of intermolecular contacts. Another example of the putative impact of inhibitor type on crystal genesis is provided by the chemical modification occurring with the 5,6-diaminouracil: the complex formed with Uox selects the *I*222 packing, the high diffraction quality of which permitted us to carry out noble-gas derivation for *ab initio* high-resolution SIR phasing and identification of the modified inhibitor. Eventually, a fourth crystal form was obtained when searching for a procedure to label cysteines with an arsenic compound for crystal derivation purposes. In Uox, two cysteines accessible to the solvent are located in the tunnel formed by the tetramer and thus are unlikely to be involved in the packing contacts. However, Uox which was complexed with an oxidized aminouracil packed in a new $P2_12_12$ crystal form involving in particular Trp174, a residue present directly or indirectly in all of the different Uox packing contacts.

Unfortunately, all of these new crystal forms (monoclinic, trigonal and primitive orthorhombic) lag behind the canonical *I*222 form in terms of diffraction quality. Neither the binding-interaction network nor the solvent-organized part could be described with similar accuracy, so little new information was obtained regarding the catalytic mechanism. Nevertheless, crystal 'pseudo-polymorphism'[1] was analysed according to the state of the active site in order to propose a correlation between stabilizing interactions within the active site and changes in non-specific intermolecular contacts.

[1] The term 'polymorphism' must be applied to the same crystal composition.

2. Materials and methods

2.1. Crystallization

Recombinant Uox from *A. flavus* expressed in *S. cerevisiae* (or rasburicase, trade name Fasturtec in the EU and Elitek in the USA) was supplied purified by Sanofi–Aventis. All inhibitors or additives used in this study (described in Fig. 2) were purchased from Sigma–Aldrich. Identical crystal-growth conditions were used as described previously (Bonneté *et al.*, 2001; Vivarès & Bonneté, 2002) using the sitting-drop vapour-diffusion method at room temperature. 5–10 mg ml^{-1} protein in 50 m*M* Tris–HCl pH 8.5 cocrystallized with any of the inhibitors (MW $\simeq$ 150 Da) in a large excess (0.5–2 mg ml^{-1}) within 24–48 h in the presence of 5–8%(*w*/*v*) PEG 8000 without attempts at pre-incubation.

In the case of 5,6-diaminouracil (m/z = 143.0 from ESI–MS), we observed that the crystallizing solutions (and subsequently the growing crystals) slowly turned yellow within a few days, probably owing to oxidation (m/z = 171 from ESI–MS, m/z = 171–172 from MALDI–MS). To prevent this instability problem and/or to accurately track down the chemical modification, crystallizations were performed under reducing conditions (1 m*M* DTT) in the presence of 100 m*M* sodium cacodylate pH 7.0 and 1 m*M* 2-aminoethyl-aminomethyl-4-(4,6-diamino-1,3,5-triazin-2-ylamino)phenylarsonodithioite, also known as cymelarsan, $AsS_2C_{13}N_8H_{21}$. These conditions were expected to derivatize the Uox–5,6-diaminouracil crystal by forming arsenic adducts with the solvent-accessible Cys35 and Cys103 on the basis of the crystallization process for the HIV-1 core domain (Maignan *et al.*, 1998), which subsequently permitted arsenic MAD structure phasing (Greenwald *et al.*, 1999). The crystallizing agent remained the same, *i.e.* 5–8%(*v*/*v*) PEG 8000 in Tris–HCl buffer.

2.2. X-ray data collection and data processing

Except for the guanine complexes, the diffraction data for which were recorded at the Cu K^{α} wavelength on a laboratory Nonius diffractometer equipped with a 345 mm MAR Research image plate, all other X-ray data collections were carried out at the DW32 station of the wiggler beamline at the LURE DCI synchrotron (Fourme *et al.*, 1992) at a wavelength of 0.972 Å using the same type of detector. Data were integrated using *DENZO* and scaled independently using *SCALEPACK*, both of which are from the *HKL* package (Otwinowski & Minor, 1997). Unit-cell parameters were refined independently by the post-refinement technique implemented in *SCALEPACK*.

The yellow *I*222 crystals that diffracted to high resolution, which were initially grown from solutions containing 5,6-diaminouracil, were subjected to strict isomorphous derivatization by pressurizing the capillary containing the crystal with noble gas. For this purpose, a complete data set to 1.6 Å resolution was first recorded from one crystal in a 'native' state (no pressure). Two gases, xenon and krypton, at respective pressures of 1 and 4 MPa were used to record two test derivative sets (resolution better than 2 Å) on two different crystals (Schiltz *et al.*, 1994, 2004). The recommendation was

Table 1
Statistics of data collection.

Urate oxidase (rasburicase) complexed with	Uracil (293 K)	5,6-diaminouracil (293 K)	5-amino-6-nitrouracil (283 K)				Guanine (293 K)	
			Native	2 MPa Xe	4 MPa Kr	Native cymelarsan		
Data collection								
Wavelength (Å)	0.972	0.972	0.972	0.972	0.972	0.972	1.5418	1.5418
Exposure time per frame (s)	120	120	160	120	180	90	360	360
Angular increment per frame (°)	1	1	1	1	1	1	1	1
Total rotation range (°)	75	220	150	139	72	169	200	191
Crystal-to-detector distance (mm)	475	440	250	280	310	390	225	170
Unit-cell parameter refinement								
Space group	$P3_121$	$P3_121$	$I222$	$I222$	$I222$	$P2_12_12$	$P2_1$	$I222$
Unit-cell parameters								
a (Å)	140.6	140.18	80.38	80.63	80.13	126.25	82.75	79.98
b (Å)	140.6	140.18	96.47	96.72	96.32	142.27	141.94	96.44
c (Å)	151.1	151.18	106.14	106.14	105.65	81.33	135.08	105.54
α (°)	90	90	90	90	90	90	90	90
β (°)	90	90	90	90	90	90	92.67	90
γ (°)	120	120	90	90	90	90	90	90
Matthews V_M coefficient (Å^3 Da^{-1})	3.24	3.20	2.80	—	—	2.75	2.99	2.88
Solvent content (%)	61.7	61.2	55.8	—	—	54.8	58.5	56.9
No. monomers per AU	4	4	1	—	—	4	8	1
Data reduction†								
No. measured reflections	129463	609595	306063	206360	83341	254790	150459	146169
Resolution limits (Å)	36.0–3.20	32.1–2.70	35–1.64	31–1.80	30–2.0	35–2.80	30–3.20	25–2.0
No. unique reflections	28902	48554	50707	38230	26878	36394	48327	26240
Data completeness (%)	99.8	99.9	99.9	98.6	96.2	98.7	93.9	94.1
In last shell	99.9	100	100	97.7	96.1	98.4	96.0	90.6
Overall $\langle I/\sigma(I)\rangle$	13.3	15.4	17.8	16.8	12.9	16.8	9.4	13.5
In last shell	9.5	9.8	10.3	9.3	9.3	10.1	5.6	9.4
Redundancy	4.4	12.5	6.0	5.3	3.1	7.0	3.1	5.5
Overall R_{sym}‡	0.093	0.087	0.037	0.046	0.058	0.069	0.114	0.134
In last shell	0.303	0.512	0.295	0.302	0.280	0.372	0.330	0.281
R_{iso}§ (20–2.00 Å)				0.135	0.127			
In last shell				0.160	0.310			
SIR phasing statistics								
R_{Cullis}¶††								
Centric				0.56 (26122)	0.84 (26973)			
Acentric				0.54 (2049)	0.81 (2204)			
Phasing power†††‡‡‡								
Centric				2.10 (26122)	0.86 (26973)			
Acentric				1.67 (2049)	0.78 (2204)			
FOM†††§§								
Centric				0.41 (27207)	0.20 (27176)			
Acentric				0.51 (2514)	0.25 (2430)			
FOM¶¶¶				0.95	0.85			
$\Delta\varphi$††† (°)				59.7	73.4			
$\Delta\varphi$‡‡‡ (°)				18.5	55.4			
Autobuilt residues (N cycles)				285 (60)	285 (90)			

† Using *SCALEPACK* except for the $P2_1$ guanine data, for which *SCALA* was used. ‡ R_{sym} is defined as $\sum_{hkl}\sum_i |I_i(hkl) - \langle I(hkl)\rangle|/\sum_{hkl}\sum_i I_i(hkl)$, where $I_i(hkl)$ is the ith observation of reflection hkl and $\langle I(hkl)\rangle$ is the weighted mean of all observations (after rejection of outliers). § R_{iso} is defined as $\sum_{hkl}|(F_{deriv}) - F_{native}|/\sum_{hkl}F_{native}$. ¶ R_{Cullis} = ⟨phase-integrated lack of closure⟩/⟨$|F_{PH} - F_P|$⟩. †† Values in parentheses are the number of reflections. ‡‡ Phasing power = ⟨$|F_H$(calc)|/phase-integrated lack of closure]⟩. §§ Figure of merit output by *SHARP* (de La Fortelle & Bricogne, 1997). ¶¶ Figure of merit output after density modification as implemented in *SHARP*. ††† Average non-weighted difference between the phases calculated from the 1wrr model and those output by *SHARP*. ‡‡‡ Average non-weighted difference between the phases calculated from the 1wrr model and those output after density modification.

followed to orient the crystal in the capillary in such a way that the incident X-ray beam and not the diffracted beams travelled through the gas atmosphere in order to minimize gas-absorption effects (Schiltz *et al.*, 1997). The merged intensity data were converted to structure-factor amplitudes by *TRUNCATE* (French & Wilson, 1978; Collaborative Computational Project, Number 4, 1994) and put on an approximate absolute scale using the scale factor taken from a Wilson plot computed with data in the resolution range to 4 Å d_{min} (see statistics in Table 1). The derivative data were scaled to the native by applying overall scale and anisotropic factors using the program *SCALEIT*.

2.3. Protein structure solutions

To ascertain the chemical composition of the yellow *I*222 Uox complex, the structure was determined *ab initio* by the SIR (single isomorphous replacement) method. Isomorphous difference Patterson maps were computed for both cases, krypton derivative/native and xenon derivative/native, and

showed one significant peak (17/5σ) in the respective Harker sections. A heavy-atom refinement and phasing strategy were carried out with the program *SHARP* (de La Fortelle & Bricogne, 1997; Bricogne, 1997). Details of the phasing output, as well as the subsequent stages comprising phase improvement and model autotracing, will be described elsewhere.

A second crystal structure of the same complex crystallized in the presence of cymelarsan was determined in a primitive orthorhombic $P2_12_12$ space group by molecular replacement with the *AMoRe* program (Navaza, 1994) using data in the 8–4 Å resolution range. The search model was the tetramer generated after applying 222 symmetry to the monomeric unit (PDB code 1r51). The rotation solution subjected to the translation function together with observed extinctions allowed us to determine two screw axes and reindex (*a*, *b*, *c* to *b*, *c*, *a*). The *R* factor reached the value of 0.318 for a correlation coefficient on *F* of 0.795 after appropriate translation of the rotation solution.

In the case of the trigonal space group $P3_121$ of the uracil–Uox and 5,6-diaminouracil–Uox complexes, the chirality of the *P*3 screw axis was determined during the search for a solution by molecular replacement using the previous 1r51 model. The first-ranked rotation solution was subjected to the translation function in *AMoRe*. The *R* factor was 0.324 with a correlation coefficient on *F* of 0.723 after a translation of 1/3 of the unit cell along *c*, whereas the values were only 0.486 and 0.495, respectively, after a 2/3 translation.

One crystal of the guanine complex was characterized as diffracting in the canonical *I*222 space group, whereas other complexed crystals belong to a fourth space group, monoclinic $P2_1$, which had already been observed for the unliganded case (Retailleau *et al.*, 2004).

All structure refinements were carried out with the program *BUSTER* (developed by Global Phasing Ltd; Irwin & Bricogne, 1996) and interfaced with *TNT* (Tronrud *et al.*, 1987). Throughout the course of each refinement, 10% of the data were left out for cross-validation ($R_{\rm free}$).

For the high-resolution *I*222 case, the starting model could have been taken indifferently from any of the complete constructions performed by the *warpNtrace* protocol within the *ARP*/*wARP* program (Perrakis *et al.*, 1999) using the accurate solvent-modified maps output by *SHARP* after running either the SIR-Xe or SIR-Kr protocol. Experimental phase information encoded as the Hendrickson–Lattman coefficients was input to constrain the model refinement. Waters and lastly the inhibitor were included subsequently from inspection of σ_A-weighted maps with $2|F_{\rm o} - F_{\rm c}|$ and $|F_{\rm o} - F_{\rm c}|$ coefficients (Read, 1986) and their atomic temperature factors were then refined. The final model held for deposit was that obtained from the SIR-Xe experiment, for reasons of better accuracy (see Table 1). Fig. 1 typically represents an omit map around the modified 5,6-diaminouracil, which was subsequently refined as 5-amino-6-nitrouracil.

Regarding the other medium-resolution structures (monoclinic, orthorhombic and trigonal), the *AMoRe* solution for each case was subjected to an initial round of rigid-body refinement of both the position and orientation of the tetramer. Residue-by-residue real-space correlation coefficients of the current model with the corresponding *SIGMAA* $2|F_{\rm o} - F_{\rm c}|$ map were checked to remove significant errors in the starting model. Manual rebuilding was performed using the program *O* (Jones *et al.*, 1991). Alternation of rounds of positional refinement on a partial free-bias model followed by manual rebuilding using *O* and rounds of grouped *B*-factor refinement were performed until model completion. Each monomer was refined independently in all cases owing to reliable starting phases and the occupancy of the ligands was estimated for each active site at the end of the refinement. Low-resolution data to 15 Å were modelled by a bulk-solvent correction using the Babinet principle as computed in *BUSTER* (Roversi *et al.*, 2000). Final statistics of the model parameter refinements are given in Table 2. For the structures of limited resolution, it was difficult to accurately model the ligands in an $F_{\rm obs} - F_{\rm calc}$ omit map centred on the cavity. Refinements suggested only partial occupancy of the active sites in the case of pyrimidines and guanine for the $P2_1$ crystal. Coordinates have been deposited in the Protein Data Bank; deposition codes are listed in Table 2.

2.4. Methods for crystal-packing analyses

The molecules are designated to be in contact if they have at least one intermolecular atomic distance less than 4.1 Å. Intermolecular contacts were examined with *CONTACT* from the *CCP*4 suite. Bound waters were left out from this analysis because water description is only available for the *I*222 structures. Areas of buried surfaces were estimated online utilizing the Protein–Protein Interaction Server (http://www.biochem.ucl.ac.uk/bsm/PP/server/; Jones & Thornton, 1996). The neighbours of Uox in a given crystal packing were generated using *O*.

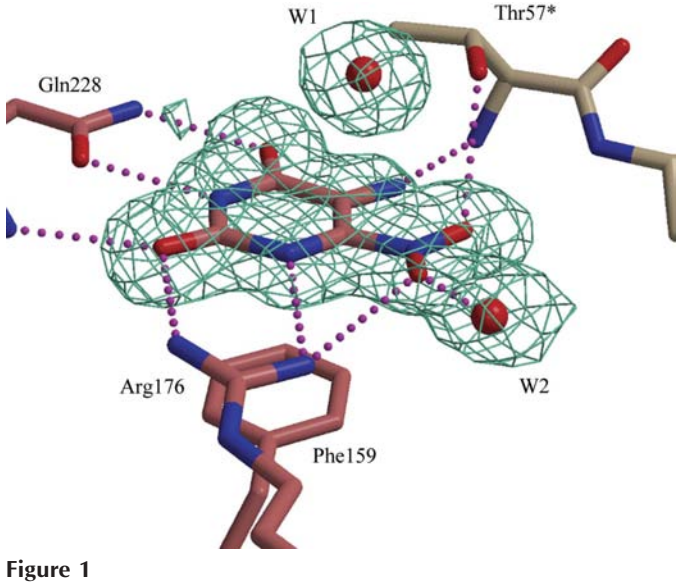

Figure 1
View of the active site: the omit map is contoured at the 1.5σ level around the 5-amino-6-nitrouracil with the model superimposed. Graphics were created using *MOLSCRIPT* (Kraulis, 1991) and rendered using *RASTER3D* (Merritt & Murphy, 1994).

Table 2
Refinement statistics.

Rasburicase in complex with	Uracil	5,6-Diaminouracil	5-Amino-6-nitrouracil		Guanine	
	$P3_121$	$P3_121$	$I222$	$P2_12_12$	$P2_1$	$I222$
No. reflections (total)	28896	47538	50756	36377	51516	26180
No. reflections ($\|F\| > 3\sigma$)	22602	40400	45314	31716	35951	20633
No. reflections for refinement	25256	37754	45173	32522	43119	23261
No. reflections used for R_{free}†	2827	4746	5052	3605	4804	2599
No. protein atoms/$\langle B\rangle$ (Å^2)						
Tetramer 1						
Monomer *A*	2363/33.0	2363/41.5	2396/20.8	2347/50.2	2359/30.9	2396/29.1
Monomer *B*	2363/33.0	2363/42.8	—	2354/49.7	2357/38.4	—
Monomer *C*	2386/33.8	2386/42.1	—	2362/43.7	2374/34.2	—
Monomer *D*	2367/33.1	2362/41.9	—	2358/46.4	2352/38.5	—
Tetramer 2						
Monomer *E*	—	—	—	—	2348/44.0	—
Monomer *F*	—	—	—	—	2349/43.8	—
Monomer *G*	—	—	—	—	2359/47.8	—
Monomer *H*	—	—	—	—	2359/41.2	—
No. water molecules (solvent)	—	58	215	26 (+ 'C6')‡	—	117
$\langle B\rangle$ for solvent molecules (Å^2)	—	33.5	34.6	35.0 (41.5)	—	36.7
Inhibitor $\langle B\rangle$/occupancy						
Tetramer 1						
Monomer *A*	43.7/0.5	33.6/0.5	22.4/1.00	39.4/1.00	39.5/0.60	22.8/1.00
Monomer *B*	46.7/0.5	32.2/0.5	—	33.0/1.00	50.8/0.50	—
Monomer *C*	45.8/0.5	42.4/0.5	—	34.1/1.00	53.2/0.45	—
Monomer *D*	42.6/0.5	32.3/0.5	—	36.2/1.00	53.2/0.45	—
Tetramer 2						
Monomer *E*	—	—	—	—	49.4/0.55	—
Monomer *F*	—	—	—	—	35.3/0.45	—
Monomer *G*	—	—	—	—	43.1/0.50	—
Monomer *H*	—	—	—	—	61.4/0.55	—
Resolution range (Å)	15–3.20	15–2.70	28–1.64	15–2.80	15–3.20	15–2.01
R value§ (%)	14.6	16.3	16.8	18.9	17.2	16.9
R_{free}† (10% reserved)	20.0	21.2	19.0	24.8	20.8	21.0
Weighted r.m.s.d. from ideality						
Bond length (Å)	0.011	0.013	0.014	0.012	0.07	0.011
Bond angle/dihedral angle (°)	1.23/19.5	1.45/19.2	1.41/13.5	1.11/19.6	0.69/18.8	1.21/17.9
Ramachandran plot: % residues in						
Most favoured regions	90.7	90.3	93.3	87.7	90.6	92.9
Additional allowed regions	9.3	9.7	6.7	12.3	9.4	7.1
PDB code	1ws3	1ws2	1wrr	1xxj	1xy3	1xt4

† The free *R* factor is a cross-validation residual calculated using 10% of the native data which were randomly chosen and excluded from the refinement. ‡ Corresponds to a phenyl group with half-occupancy factor, assumed to lie on the dyad axis. § The crystallographic *R* factor is defined $\sum |F_o| - |F_c|/\sum |F_o|$ and indicates the accuracy of the model.

3. Results and discussion

3.1. Four crystal forms for Uox depending on the type of inhibitor

Original work on Uox crystallization was carried out systematically on an extracted enzyme in the presence of 8-azaxanthin, a competitive inhibitor (Colloc'h *et al.*, 1997). Subsequent structural investigation on the enzymatic oxidative mechanism of Uox benefitted from the crystallization studies conducted by Bonneté and coworkers (Bonneté *et al.*, 2001; Vivarès & Bonneté, 2002), which aimed at rationalizing and predicting nucleation and crystal-growth conditions for Uox. Long-chain polymers such as PEG 8000 and rather basic pH were determined to be very beneficial for Uox crystal production. In the meantime, a new preparation of Uox provided us with a supply of recombinant enzyme that was largely inhibitor-free and highly pure (Bayol *et al.*, 2002). Previously used conditions were succesfully applied to the crystallization of either ligand-free or other inhibitor-complexed Uox (Fig. 2). Therefore, the variation in crystal forms could be inferred as mainly related to the choice of chemicals present in the medium and interacting in the active sites.

The strategy for structural study of an enzymatic mechanism aims at trapping the enzyme both in the ground state and transition states. Cocrystallization with a compound that can mimic the substrate is a primordial stage to fill the enzyme active site. For this purpose, analogues which closely resemble uric acid, the natural substrate, such as 8-azaxanthin, 9-methyluric acid or oxonic acid (Fig. 2), were tested with priority. The good diffraction properties of the resulting diamond-shaped *I*222 crystals could be perceived as a confirmation that these molecules were good analogues. In guanine, the substitution of a carbonyl by an amine group in the six-membered ring leads to the genesis of needle-like or thin elongated plate-shaped crystals, a sign of a possible weakening in intermolecular recognition. Indeed, these crystals belong to a primitive monoclinic array, $P2_1$, in which the free enzyme had previously been shown to crystallize (Retailleau *et al.*, 2004). This form diffracts less effectively than the *I*222 form

(to about 2.3 Å) with noticeable crystal decay on exposure to X-rays. Intriguingly, one large parallelepiped crystal grew amongst the elongated crystals and was identified to belong to space group *I*222.

The use of pyrimidine-like inhibitors (*e.g.* uracil or 5,6-diaminouracil) led to the formation of a third form, which was characterized as trigonal. The diffraction properties of these crystals were even poorer than those of the preceding ones (around 3 Å), confirming that complexation for cocrystallization is best ensured with a chemical that is closely analogous to the real substrate.

The list of Uox crystal forms induced by the presence of additives may not be exhaustive. We report here a fourth form which also binds oxidized aminouracil but which grew in the presence of cymelarsan, a compound that is not supposed to inhibit the enzyme. Instead, this compound was expected to react covalently with cysteines present on the inner face of the enzyme tunnel. This form belongs to the orthorhombic family but unlike the original body-centred space group has a primitive cell with two screw axes ($P2_12_12$) and diffracts more weakly (2.8 Å).

To a first approximation, the four crystal forms have equivalent (60 ± 3%) solvent contents that cannot exclusively account for the observed discrepancies in diffraction limits (see Table 1), even if the highest value is associated with the poorest diffracting trigonal form. Thus, the explanation should be found in the analysis of each asymmetric unit content (subunits obeying either crystallographic or non-crystallographic symmetry) and of their packing in the respective lattices.

When uric acid analogues bind to Uox, the resulting *I*222 crystal is built up from the repetition of one monomer (the fourth of the enzyme) throughout the crystal volume, whereas in the other cases the asymmetric units contain either one ($P3_121$, $P2_12_12$) or two ($P2_1$) tetramers with potentially four or eight independent monomers. This introduces a larger number of degrees of molecular freedom, which inevitably causes additional disorders in the crystal (see §3.3 for packing analysis).

Selection of one of these space groups was partially addressed in terms of the capacity of the ligands to stabilize the active site and the entire molecule by extension (see §3.4 for a discussion of inhibitor binding). A close analogue uniformly stabilizes the active sites, rendering the tetramer perfectly symmetric, which in turn favours regular contacts in the crystal and contributes to higher intrinsic order, as also reflected by the high-resolution diffraction power.

3.2. Comparisons of Uox structures from the different space groups

Despite the different manners in which the four crystal systems pack, the molecules display relatively minor differences in their structures compared with those previously reported (Retailleau *et al.*, 2004). The rasburicase model comprises 295 amino acids per monomer out of a total of 301 (with the N-terminus acetylated) in orthorhombic space groups. In the trigonal and monoclinic forms and despite the lower resolution, three of the six last C-terminal residues were revealed (Ser296, Leu297 and Lys298) owing to packing stabilizations. Rasburicase has three cysteines per monomer; two of them, Cys35 and Cys103, are accessible to the solvent, whereas the third one, Cys295, is buried but displays a dual

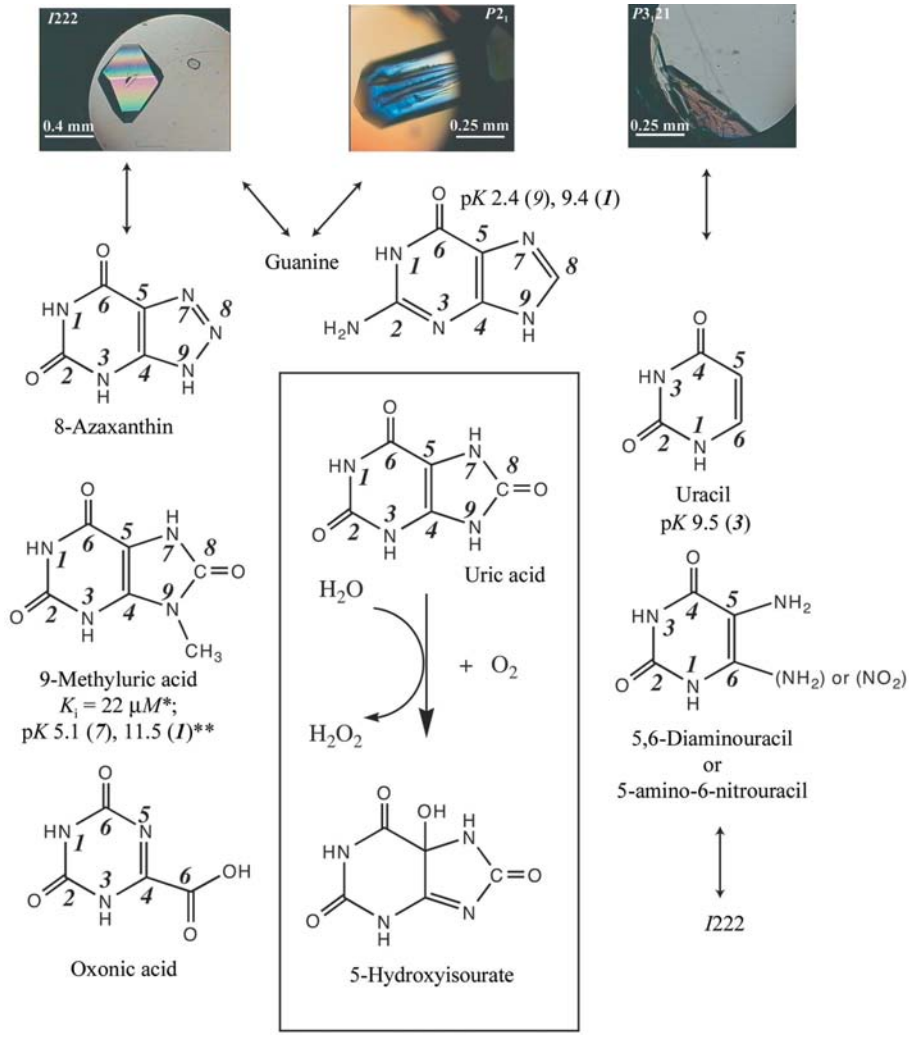

Figure 2
The reaction pathway from uric acid to 5-hydroxyisourate (middle) and the analogues used. Note that uracil (and derivatives) standard numberings differ compared with uric acid derivatives. *, Kahn & Tipton (1997); **, Pfleiderer (1974).

position for the S atom pointing either toward the side chains of Met231 and Val292 or Val3*[2] at the dimer interface. In the orthorhombic $P2_12_12$ structure, an extra density restricted to one atom size is observed in all the monomers at the extremity of the side chain of both Cys35 and Cys103. Expectations of an arsenic adduct from the cymelarsan are not favoured owing to the absence of even weak anomalous signal in an anomalous Fourier synthesis (~2.9 e^- at λ = 0.97 Å). Formation of disulfide bridges arising from the presence of DTT remains the most likely explanation. In the original structure of extractive urate oxidase (Colloc'h *et al.*, 1997), a free cysteine from the solvent was involved in a disulfide bridge with Cys35, showing that this cysteine is particularly reactive.

Average displacements in the main chains of the different protomers for the respective complexes are reported in Fig. 3(*a*). Owing to small variations between protomers, averaged coordinates for each case are held for superposition on the monomer determined from the *I*222 high-resolution crystal. The r.m.s. deviations in main-chain positions in all cases remain remarkably small (within 0.4 Å), despite the lack of accuracy for most of the models. However, tetramers can be divided into two groups of structures since the r.m.s. displacements in the main-chain positions between those in the orthorhombic family on one hand and those in the monoclinic and trigonal families on the other are significantly smaller than the cross values (Fig. 3).

The region that mainly accounts for significant changes in the backbone positions between the two groups of structures (maximum r.m.s. displacement of 1.5 Å) is the loop that encompasses the residues in the vicinity of the active site (Figs. 3 and 6) owing to the different inhibitor sizes and characteristics.

In the 5-amino-6-nitrouracil–Uox structure, the water molecules (a total of 215) introduced in the *I*222 SIR model basically correspond to those present in previously deposited structures. In contrast, only a handful of waters involved in a strong hydrogen-bonding network were included in the non-*I*222 final models, while the solvent part was omitted from the structures refined at 3.2 Å. The two molecules W1 and W2 (Fig. 1) that are assumed to play a role in the catalytic reaction are always observed in the high-resolution electron density derived from the *I*222 crystals. W2 lies very close to $O^{\delta1}$ in the extremely electrophilic nitro group (~2.2 Å). Surprisingly, no significant density for W2 could be seen in the vicinity of this group in the primitive orthorhombic case, probably because of the poorer diffraction quality of the $P2_12_12$ crystal. W1, which bridged the side chains of Asn254 and Thr57* in the previously deposited models (1r51, 1r4s, 1r4u), is observed above both the guanine ring in the *I*222 structure and the 5-amino-6-nitrouracil in both orthorhombic structures. However, W1 is missing above the 5,6-diaminouracil single ring because these two side chains are moving apart in the trigonal space group (Fig. 3*b*).

3.3. Packing contacts in the four crystal lattices

The four different crystal packings are illustrated in Fig. 4 and their contact zones represented as *GRASP* (Nicholls *et al.*,

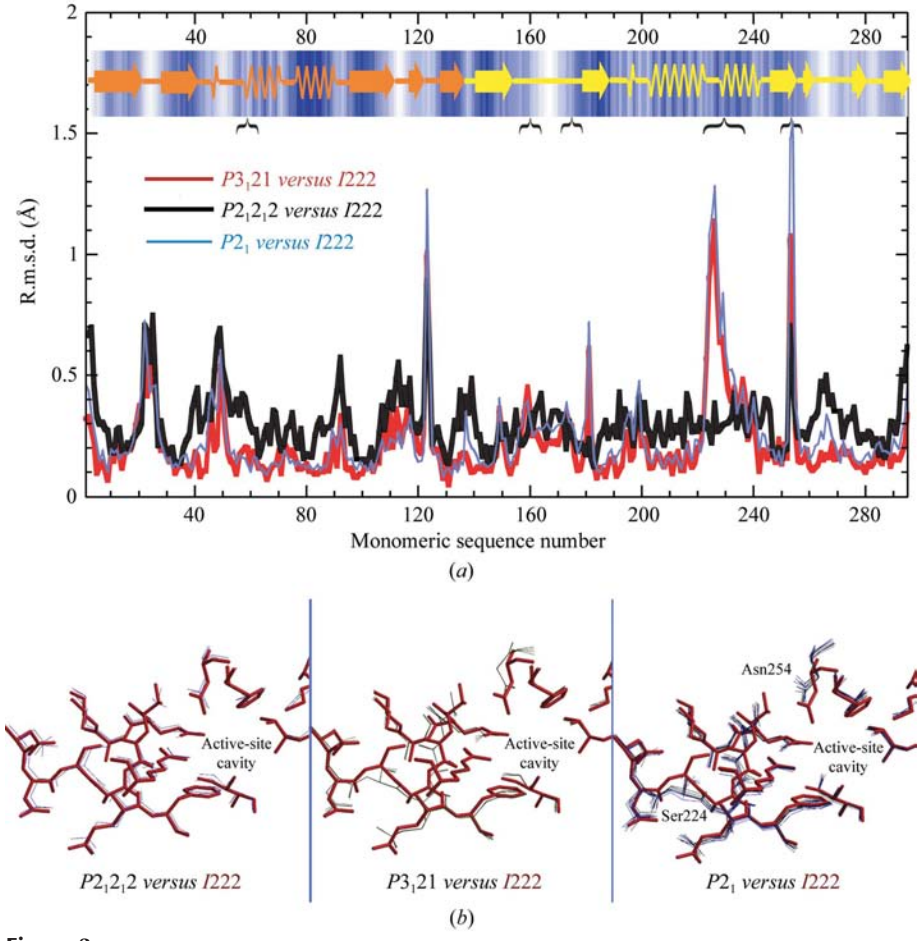

Figure 3
(*a*) Monomeric sequence analyses of r.m.s. coordinate differences for main-chain atoms between the *I*222 high-resolution structure taken as reference (PDB code 1wrr) and protomers from the other packings (PDB code 1ws2 for the trigonal case). Coordinates are averaged by the number of protomers per AU in each different space group after superimposition on the reference set. This was made possible by the small r.m.s differences between the protomers in each quaternary structure. The secondary structure is displayed as an insert (the central motif is coloured as follows: orange, first domain; yellow, second domain; white background, solvent-accessible residues; blue background, buried residues, as estimated by *PROCHECK*). The curved brackets refer to the residues which line the active-site region. (*b*) Close-up view of that region after superimposition of all the copies per AU for each case over the *I*222 reference.

[2] * indicates another monomer, whether symmetry-related or not.

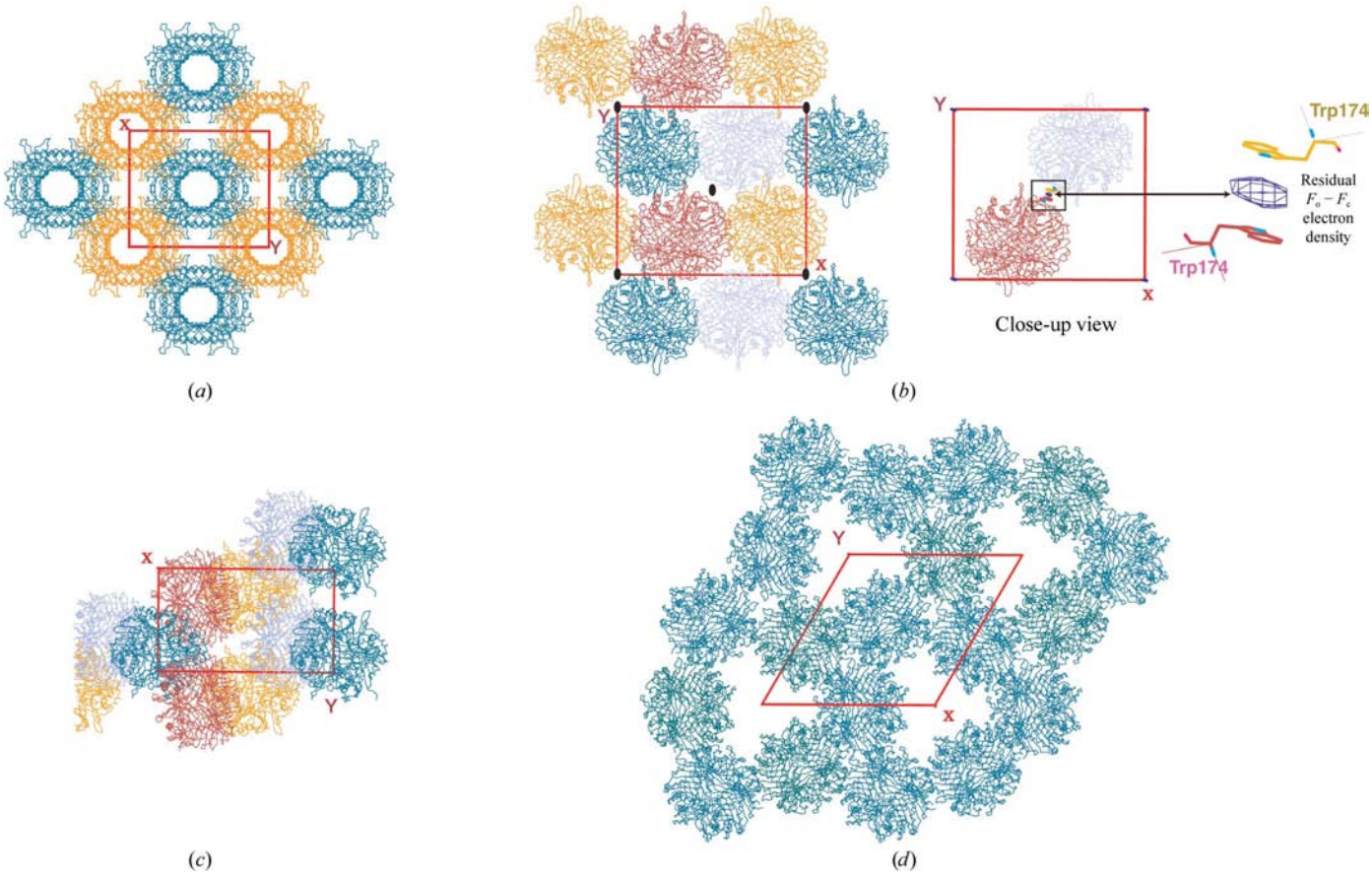

Figure 4
Packing of the different crystal forms: (*a*) *I*222, (*b*) $P2_12_12$, (*c*) $P2_1$, (*d*) $P3_121$.

1991) surfaces with interacting residues labelled are in Fig. 5. All the different contacts are individually listed in the supplementary material[3].

3.3.1. Orthorhombic *I*222 form. This is the most common crystal form of this enzyme, with one monomer in the AU. The biologically functional tetramer consists of the monomer *A* in a general position (x, y, z), which corresponds to the asymmetric unit, and monomers *B*, *C* and *D* in positions ($1 - x$, $1 - y$, z), (x, $1 - y$, $1 - z$) and ($1 - x$, y, $1 - z$), respectively. Each tetramer is placed at a 222 symmetry site of the body-centred space group. Therefore, each tetramer is surrounded by eight other tetramers related by the *I*-centring of the cell: $x \pm 1/2$, $y \pm 1/2$, $z \pm 1/2$ (see Fig. 4*a*). Strikingly large channels measuring 12 Å in diameter and smaller ones with a diameter of less than 10 Å run parallel to the *c* axis through the entire crystal. The larger channels correspond to the perfect alignment of the 50 Å long inner tunnels built by the tetramer. In addition to the contacts related to the dimer interface with *B* (surface of ∼2900 Å^2) and tetramer interface with *C* (surface of ∼2650 Å^2), each monomer generates three zones of contact (termed macrobonds) with counterparts (Fig. 5*a*) covering a total surface of 420 Å^2. These zones are located in the regions formed by residues 4–51, residues 195–198 and residue 160 plus residue 225. The contacts are essentially of van der Waals type; none of the distances of the hydrogen bonds reported in the supplementary material[3] are less than 3.6 Å.

3.3.2. Orthorhombic $P2_12_12$ form. This primitive orthorhombic form differs completely in the arrangement of the tetramers (Fig. 4*b*). One complete tetramer now corresponds to the content of the AU. The independent tetramer is surrounded by 12 other congeners, but only eight of them make close contacts with the reference molecule in general position (x, y, z). The tunnels of the tetramers are no longer aligned along a particular crystal axis. The contact regions in *I*222 are however conserved in the primitive orthorhombic packing, accounting for less than a third of the total surface contact. As a consequence, after a 90° rotation the tunnels of symmetry-related molecules in positions x, y, $z \pm 1$ and those in position $x \pm 1/2$, $1/2 - y$, $-z$ are aligned with that in position x, y, z. Fig. 5(*b*) shows the two new main contact zones arising from the $P2_12_12$ packing and involving polar interactions. The first contact zone brings together the region which encompasses Glu89, His95 and Glu136–Lys138 and that which comprises Gln158 and Asn223. The second contact zone implicates the N-terminal region from monomer C and Glu236–Gln243 from monomer *D*. This wide distribution of

[3] Supplementary data have been deposited in the IUCr electronic archive (Reference: TM5013). Details for accessing these data are given at the back of the journal.

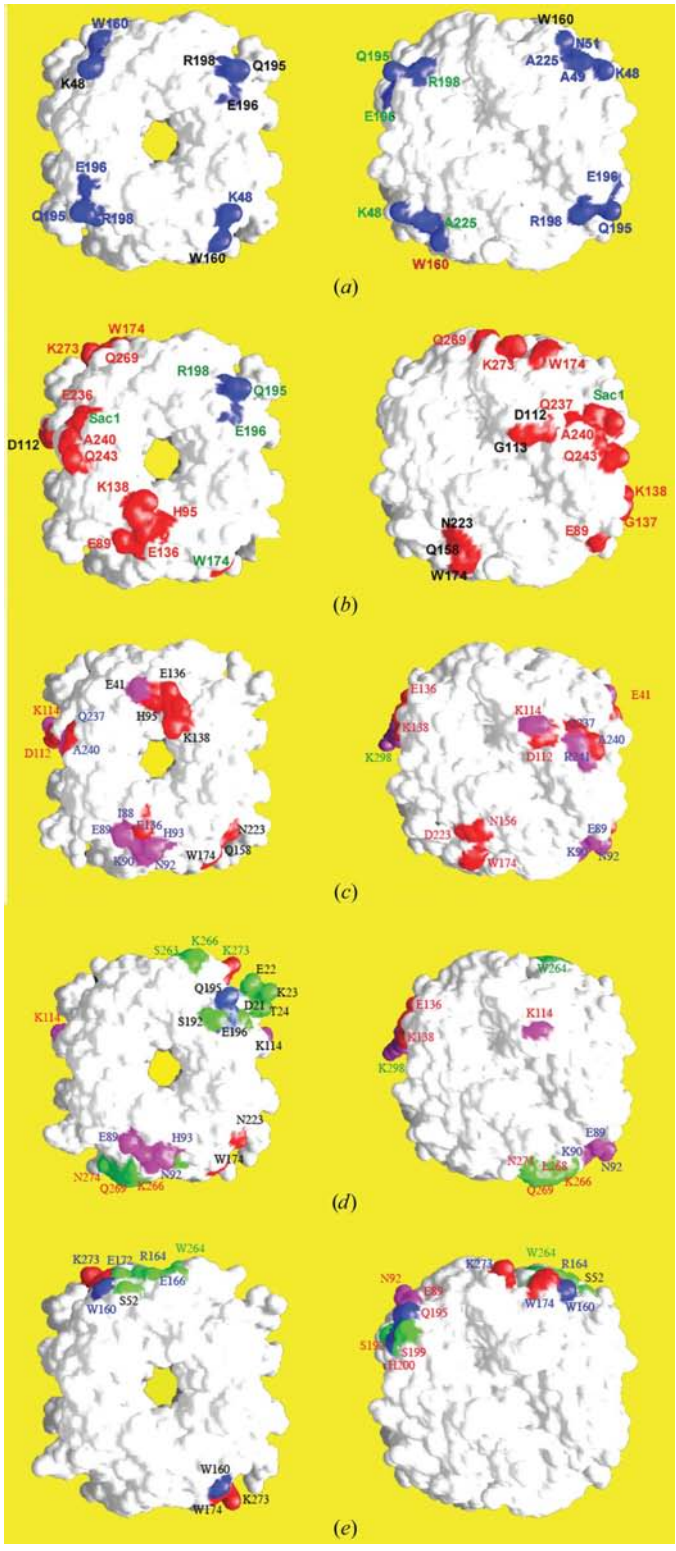

Figure 5
Two orthogonal views of Uox tetramers showing the zones involved in packing contacts (drawn using *GRASP*; Nicholls *et al.*, 1991). Colour codes are as follows. Labels: black labels refer to residues in monomer *A* (or *E*), blue those from monomer *B* (or *F*), green monomer *C* (or *G*) and red monomer *D* (or *H*). Contact surfaces: blue show the contact zones in the canonical *I*222 packing; red the common zones in $P2_12_12$, $P3_121$ and $P2_1$, magenta the contact zones common to $P3_121$ and $P2_1$ and green the contact zones specific to the $P2_1$ packing. (*a*) *I*222, (*b*) $P2_12_12$, (*c*) $P3_121$, (*d*) $P2_1$ (a), (*e*) $P2_1$ (b).

contact zones around the tetramer leads to an oblique (90°) orientation of the four other contacting barrels relative to the reference molecule with respect to the *c* axis.

However, a striking observation of a flat residual electron density in the final refined map was made exactly at the twofold *c* axis and stacking between two tryptophans, Trp174 and its twofold counterpart (inset in Fig. 5*d*). The nature of this necessarily twofold symmetric compound lying on a special position might correspond to degradation of the cymelarsan additive into a phenyl or triazine moiety, or to pyrimidines from the crystallizing medium. In any case, the presence of a flat-ring compound in the electron density is definitely responsible for inducing the peculiar molecular arrangement. The importance of solvent molecules in promoting Uox contacts has also been oberved recently with another source of Uox (from *Bacillus sphaericus*), which crystallized in complex with 8-azaxanthin in the same $P2_12_12$ space group (Hibi *et al.*, 2005; PDB code 1j2g). *B. sphaericus* Uox (which is 20 residues longer but shares about 23% strict sequential identity with *A. flavus* Uox) displays very high structural identity with the tetrameric *B. sphaericus* Uox–AZA structure (PDB code 1r51) and the crystallization conditions are the same except for a supplement of Li_2SO_4, which seems to make the difference. Indeed, sulfates were found at the interface of certain molecular pairs in the crystal packing, interacting in particular with arginine or lysine side chains. Surprisingly, the barrel-shaped tetramers packed almost as in the *I*222 structure with their tunnels aligned along the *c* axis and surrounded by eight tetramers (but six of them lie particularly close to the reference molecule).

Nevertheless, Trp174 seems to be more than anectodal at the Uox surface since it appears to be the unique residue participating in crystal contacts in the four lattices, assuming that its indole group in shifted stacking with that of Trp160 also contributes to contacts in *I*222 packing.

Regarding the compactness of internal fourfold symmetry and the variety of patches over a large accessible surface, it is not surprising that some molecular rotations offer other ways to obtain suitable close crystal arrangements. The following description of two further Uox crystal forms demonstrates that potential combinations of molecular rotation and translation in the crystal are effective.

3.3.3. Monoclinic $P2_1$ form. In the monoclinic cell, there are two tetramers per AU; each tetramer is surrounded by 12 congeners (including the second tetramer in the AU), but one makes close contact with eight of them and the second tetramer in the AU makes contact with only four, suggesting a rather inhomogeneous distribution of molecules within the crystal packing.

Common contacts with the primitive orthorhombic structure owing to the conservation of a twofold screw axis along the *b* direction are the zone around Asp112 and Trp174 on the other side of the barrel and the contacting zone involving Trp174 and the patch (Glu136, His95 and Glu41) (Figs. 5*d* and 5*e*; zones in red). Two enzyme regions that are disordered in the orthorhombic systems were modelled more accurately owing to stabilizing interactions that have developed in the

new packing: the loop 20–24 from monomer *A* lies over two indole groups, Trp160 and Trp174, from monomer *F* ($-x$, $y + 1/2$, $1 - z$) and the C-terminal region of monomer *C* is wedged between the two tetramers of the AU in position ($-x$, $y + 1/2$, $1 - z$), making all but the C-terminal residues Lys300 and Leu301 now observable.

3.3.4. Trigonal $P3_121$ form. One tetramer of the asymmetric unit makes close contacts with five other molecules. Unlike the *I*222 packing, the orientations of the barrels are in the plane perpendicular to the *c* axis and are arranged in a circular association around each trigonal axis, thus creating large solvent channels, approximating a triangular section, that run parallel to the *c* axis throughout the length of the crystal (Fig. 4*d*). Fig. 5(*c*) shows that the contacts between the tetramers are less important and are distributed only in particular regions on both sides of the barrels. All other residues are exposed to the solvent.

By analogy with the close r.m.s. coordinate differences between the $P3_121$ and $P2_1$ skeletons, the present contact zones recall most of those observed in the previous $P2_1$ packing (Fig. 5*d*). Additionally, the C-terminal portion of one monomer has also been extended to Ser299. Also common to the two independent $P2_1$ tetramers is the Glu89–His93 contacting patch.

In terms of buried surface areas involved in the crystal contacts, all forms display approximately the same surface around 1800 Å^2, which represents less than 5% of the tetramer ASA (∼45 500 Å^2). However, the $P2_1$ case presents the most compact packing around one monomer (*A*), which makes a contact surface greater than 2200 Å^2 with its eight closest neighbours, whereas the second monomer in the AU displays only ∼1300 Å^2. In contrast, the contact zones in *I*222 appear to cover the smallest surface. Given that the best diffraction properties are associated with this form, stability of packing cannot be judged in terms of surface dimensions but rather in terms of how well any space group can accommodate the oligomer symmetries as part of the crystal symmetry.

In contrast with the polymorphism of thaumatin (Charron *et al.*, 2004) or lysozyme, which are proteins of external surface four to seven times smaller than that of Uox, about only about a fifth of the latter area, was recruited to generate four different polymorphs whereas 'almost any place on the surface of the [previous] systems is involved in one or another contact in one of the four observed crystals' (Matsuura & Chernov, 2003). The question that could be addressed is whether Uox, as a large globular macromolecule, behaves differently from the previous test cases or whether we can expect to find further crystal forms upon variation of the crystallization conditions.

3.4. Inhibitor binding

The binding sites are depicted in Fig. 6. The active site is located at the dimeric interface between the two subunits that build the central tunnel. All the compounds found their way into the deep crevice formed at this dimer interface, which opens towards the exterior of the tetramer.

It is known from the previous Uox structures that the side chains of Gln228 and Arg176 are the two arms of the tweezers that hold the substrate *via* N1···O6 and O2···N3 hydrogen bonds, respectively (Retailleau *et al.*, 2004). It is likely that the same recognition takes place for the pyrimidines, which correspond to the six-membered ring moiety of the substrate. Hydrogen-bond distances are nevertheless particularly long and the stacking over Phe159, especially in the case of uracil, appears disordered. The absence of the five-membered ring prevents them from interacting with residues of the second subunit involved in pocket formation. Together, these observations may explain the weak binding and destabilization of the active site that leads to a low-resolution crystal form.

Additionally, the eight active sites that compose the asymmetric unit for the complex with guanine cocrystallized in the monoclinic form were treated as independent and partial occupancy for each ligand was estimated taking care that the

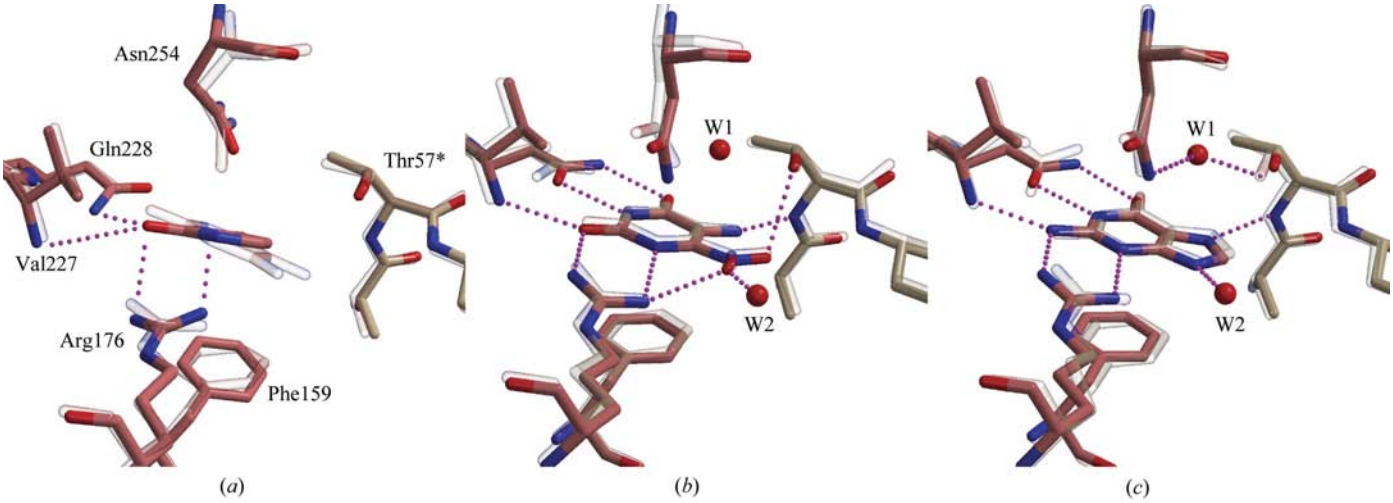

Figure 6
Positions of the different inhibitors within the active site of Uox: (*a*) uracil and 5,6-diaminouracil (in transparency); (*b*) 5-amino-6-nitrouracil in *I*222 and in $P2_12_12$ (in transparency); (*c*) guanine in *I*222 and $P2_1$ (in transparency).

respective grouped *B*-factor values matched those of the neighbouring residues. The substitution of O2 by N2 may weaken the hydrogen bond to the guanidinium group of Arg176.

The conclusion can be drawn that the closer to uric acid the analogues are, the more stabilized the dimer interface located around the active site is. This is effective directly *via* interactions with the tweezers on one side and Thr57* and Asp58* on the other side and indirectly *via* the water above the ligand plane bridging Asn254 and Thr57*. In consequence, an optimized stabilization of the quaternary structure can be assessed by the formation of highly ordered crystal packing, *e.g. I*222.

Such a result highlights the correlation between the design of inhibitors to efficiently bind to the enzyme and the quality of structural information that can be usefully derived from crystallography. In this context, the next investigation will consist of site-directed mutagenesis. We suspect that mutation of residues involved in the ligand recognition will destabilize the tetramer and lead to one of these new crystal forms.

4. Conclusion

In the present study, we report the pseudo-polymorphism of Uox crystals by describing two new crystal structures that differ from both pre-existing forms (unliganded $P2_1$ and complexed *I*222 structures). Uox crystallizes as a functionally globular homotetramer in all these space groups and besides a small movement of a region next to the active site, its main-chain structure is strictly conserved in all four crystalline lattices. Except in the case of the $P2_12_12$ form, which is likely to be related to a side effect from the crystal-growth medium, only additives interacting with the enzyme activity seem to be responsible for the polymorphism. This appears to be a singular example with respect to frequently observed cases in which polymorphism arises either from variations of major usual parameters known to affect crystal growth (temperature, pH, precipitant salts or crystallizing reagents) or from important conformational changes in modular proteins in response to ligand binding. It is now well accepted and quantified that the 'strength of macrobonds in protein crystals is one of the weakest of the protein-interaction systems' (Matsuura & Chernov, 2003) and therefore packing modification can be seen as a response to small changes at a single inner position of the protein. In our case, the active site at the dimeric interface is connected to a tunnel built by the arrangement of all subunits. It thus also influences the other interfaces (also called the tetrameric interface). This may explain the variety of Uox crystals and may also serve to address questions about intramolecular interactions that might exist in a biological assembly comprising several suspected communicating active sites (Dasgupta *et al.*, 1997).

It turns out that the closer from the natural substrate the inhibitor is with respect to a steric and chemical standpoint, the greater the tetrameric conformation is stabilized by developing tighter interactions at the dimer interface where the ligands lie. Such a low-energy conformation is associated with a crystal lattice of high order, contributing to the best diffraction. It is therefore necessary to bear this observation in mind when designing inhibitors for structural investigation around the enzyme transition state.

The ability of Uox to pack in different crystal lattices provides a good test case for high-pressure experiments to check whether application of very high pressure constraints to low-diffraction crystal forms favours crystal transition to a better order as has been observed in some cases (Fourme *et al.*, 2002) or may compress the quaternary structure along a particular direction that might be particularly evident in the case of the *I*222 crystal.

This work was partly supported by European Commission Grant No. HPRI-CT-1999-50015 within the EXMAD project. We thank Sanofi–Aventis for supplying us with pure enzyme. We thank Global Phasing Ltd for licenses for *SHARP* and *BUSTER*/*TNT* and particularly G. Evans and P. Roversi for help with low-resolution structure refinement. We also thank O. Bertrand (INSERM, Paris) and J. G. Wolf (Toulouse) for a gift of cymelarsan and A. A. Aplin (Albany Medical College) for proofreading the manucript. We thank C. Girard and V. Guérineau (Mass Spectrometry Laboratory, ICSN-Gif) for carrying out mass-spectroscopy experiments.

References

Alvares, K., Widrow, R. J., Abu-Jawdeh, G. M., Schimdt, J. V., Yeldani, A. V., Rao, M. S. & Reddy, J. K. (1992). *Proc. Natl Acad. Sci. USA*, **89**, 4908–4912.
Bayol, A., Capdevielle, J., Malazzi, P., Buzy, A., Bonnet, M. C., Colloc'h, N., Mornon, J. P., Loyaux, D. & Ferrara, P. (2002). *Biotechnol. Appl. Biochem.* **36**, 21–31.
Bonneté, F., Vivarès, D., Robert, C. & Colloc'h, N. (2001). *J. Cryst. Growth*, **232**, 330–339.
Bricogne, G. (1997). *Methods Enzymol.* **276**, 361–423.
Charron, C., Giegé, R. & Lorber, B. (2004). *Acta Cryst.* D**60**, 83–89.
Collaborative Computational Project, Number 4 (1994). *Acta Cryst.* D**50**, 760–763.
Colloc'h, N., El Hajji, M., Bachet, B., Lhermite, G., Schiltz, M., Prangé, T., Castro, B. & Mornon, J. P. (1997). *Nature Struct. Biol.* **4**, 947–952.
Dasgupta, S., Iyer, G. H., Bryant, S. H., Lawrence, C. E. & Bell, J. A. (1997). *Proteins Struct. Funct. Genet.* **28**, 494–514.
Fourme, R., Ascone, I., Kahn, R., Mezouar, M., Bouvier, P., Girard, E., Lin, T. & Johnson, J. E. (2002). *Structure*, **10**, 1409–1414.
Fourme, R., Dhez, P., Benoit, J. P., Kahn, R., Dubuisson, J. M., Besson, P. & Frouin, J. (1992). *Rev. Sci. Instrum.* **63**, 982–987.
French, G. S. & Wilson, K. S. (1978). *Acta Cryst.* A**34**, 517–525.
Greenwald, J., Le, V., Butler, S. L., Bushman, F. D. & Choe, S. (1999). *Biochemistry*, **38**, 8892–8898.
Hibi, T., Nago, T., Nishiya, Y. & Oda, J. (2005). In preparation.
Irwin, J. & Bricogne, G. (1996). *Acta Cryst.* A**52**, C86.
Jones, S. & Thornton, J. M. (1996). *Proc. Natl Acad. Sci. USA*, **93**, 13–20.
Jones, T. A., Zou, J. Y., Cowan, S. W. & Kjeldgaard, M. (1991). *Acta Cryst.* A**47**, 110–119.
Kahn, K. & Tipton, P. A. (1997). *Biochemistry*, **36**, 4731–4738.
Kraulis, P. E. (1991). *J. Appl. Cryst.* **24**, 946–950.
La Fortelle, E. de & Bricogne, G. (1997). *Methods Enzymol.* **276**, 472–494.
Maignan, S., Guilloteau, J. P., Zhou-Liu, Q., Clement-Mella, C. & Mikol, V. (1998). *J. Mol. Biol.* **282**, 359–368.
Matsuura, Y. & Chernov, A. A. (2003). *Acta Cryst.* D**59**, 1347–1356.

Merritt, E. A. & Murphy, M. E. P. (1994). *Acta Cryst.* D**50**, 869–873.
Navaza, J. (1994). *Acta Cryst.* A **50**, 157–163.
Nicholls, A., Sharp, K. & Honig, B. (1991). *Proteins*, **11**, 281–296.
Otwinowski, Z. & Minor, W. (1997). *Methods Enzymol.* **276**, 306–326.
Perrakis, A., Morris, R. J. & Lamzin, V. S. (1999). *Nature Struct. Biol.* **6**, 458–463.
Pfleiderer, W. (1974). *Liebigs Ann. Chem.* **12**, 2030–2045.
Raychaudhuri, A. & Tipton, P. A. (2003). *Biochemistry*, **42**, 6848–6852.
Read, R. J. (1986). *Acta Cryst.* A**42**, 140–149.
Retailleau, P., Colloc'h, N., Vivarès, D., Bonneté, F., Castro, B., El Hajji, M., Mornon, J. P., Monard, G. & Prangé, T. (2004). *Acta Cryst.* D**60**, 453–462.
Roversi, P., Blanc, E., Vonrhein, C., Evans, G. & Bricogne, G. (2000). *Acta Cryst.* D**56**, 1316–1323.
Schiltz, M., Fourme, R. & Prangé, T. (1994). *J. Appl. Cryst.* **27**, 950–960.
Schiltz, M., Fourme, R. & Prangé, T. (2004). *Methods Enzymol.* **374**, 83–119.
Schiltz, M., Shepard, W., Fourme, R., Prangé, T., de La Fortelle, E. & Bricogne, G. (1997). *Acta Cryst.* D**53**, 78–92.
Tronrud, D. E., Ten Eyck, L. F. & Matthews, B. W. (1987). *Acta Cryst.* A**43**, 489–501.
Vivarès, D. & Bonneté, F. (2002). *Acta Cryst.* D**58**, 472–479.